THE PREDICTION OF LIFT INFERRED FROM DOWNSTREAM VORTICITY MEASUREMENTS

W. Send
DFVLR-Institute of Aeroelasticity
Göttingen, Fed. Rep. of Germany

Abstract

A new method is presented to investigate wakes in wind tunnel tests and to predict lift distributions from downstream vorticity measurements. Its application covers the wide range from fixed wings to rotating systems; it is not bound by the need for the mathematical modelling of a given configuration. The prediction of lift is based theoretically on a relation between the running-time shift of an ultrasonic pulse passing the wake and the vorticity contained in it. Mathematical models of selected flow fields allow the theoretical simulation of wind tunnel tests and give some insight into the applicability, accuracy and limitations of the method. Preferred applications are comparative measurements of tip shapes or the investigation of rotor wakes. Compared with point-to-point measurements in a flow field, e.g. by laser anemometry, the method provides integral values in thin and sensitive regions (such as vorticity in the wake). The relation between running time and vorticity is derived. Two steps of approximation relate the shift in running time to steady and unsteady downstream vorticity and finally to spanwise lift distribution. Crosswise arrangement of running-time measurements permits wake formation in fixed and rotating blades to be traced.

I. Introduction

The investigation of flow patterns by means of ultrasonic pulses in steady flow was introduced by D.W. Schmidt[1] and was continued by R.H. Engler[2]. The method was extended to include measurements in unsteady flow for the first time by W.J. Wagner, R.H. Engler and B. Weitemeier[3] in 1980. The technical background and some initial applications were published in 1982[4].

Running-time measurements were part of an investigation concerning various blade tip shapes of rotor blades. The results were intended to give a better understanding of vorticity formation and concentration in the wake of a blade. The experiments have been performed in recent years at our research centre and also included unsteady pressure measurements[5]. The particular aim of the theoretical research was a deeper understanding of vorticity production on a lifting surface and an appropriate description of convected vorticity in unsteady flow.

The velocity field induced by the downstream vorticity determines the typical shape of the running-time signals. The mathematical model applied to describe the three-dimensional flow around a profile of finite thickness is a higher-order panel method[6]. The physical assumptions for the fluid are infinitely high Reynolds number and incompressible flow, which lead to a simplified vorticity transport equation. Harmonically varying motion produces harmonically varying vorticity. An essential part of the theory is the analytical solution of the three-dimensional wake integral in unsteady flow permitting fast and precise computation of induced velocity fields[7],[8]. The theory describes running-time measurements in front of a profile as well as downstream[9] of it.

The present paper extends the method of ultrasonic pulse measurements to measurements of vorticity. The running time is mathematically a well-defined function in the flow field and its gradient may be related to the vorticity density along the path of the signal.

II. Running-Time Shift

An ultrasonic pulse passing the flow around a wing experiences a typical shift of its running time which will be discussed at first.

For any point $\vec{r}$ in the flow field and any time t the relative velocity with respect to the wing may be described by

$$\vec{v}_{rel}(\vec{r},t). \qquad (1)$$

A pulse transmitted at a point $\vec{r}_T$ into a direction $\vec{n}(\vec{r}_T,t)$ is initially propagated at a velocity

$$\vec{v}_{rel}(\vec{r}_T,t) + c_S\,\vec{n}(\vec{r}_T,t) \qquad (2)$$

where c_S is the local velocity of sound. The first assumption we make is that of a constant velocity of sound throughout the fluid. The assumption is equivalent to an almost constant temperature in a wind tunnel. The drift of temperature during a long operating time of the tunnel has to be considered as a time-dependent correction of c_S.

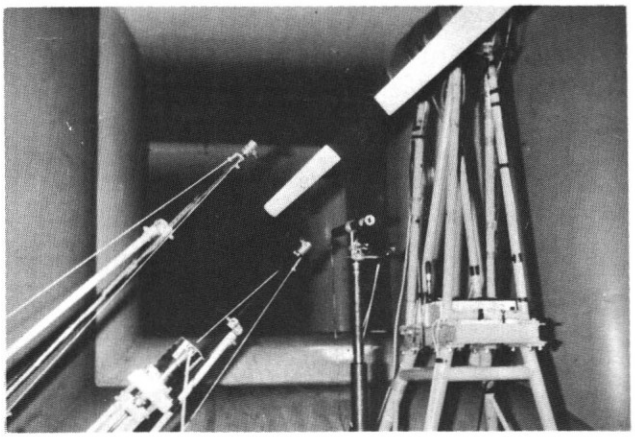

Figure 1. Transmitter and receiver (with the blade in between)

The signal is convected by the fluid; its position after a given time interval basically results from an integration of the velocity in Eq. (2) and therefore is unknown in advance. However, as long as the relative velocity is small compared to the velocity of sound, the final position may be estimated quite accurately. In addition the pulse widens during its passage through the fluid and finally covers an area large enough to be detected. We approximate the path of the signal by a straight line and prescribe the point $\vec{r}_R$, where the signal is supposed to be received by a microphone. The given spatial distance

$$D = |\,\vec{r}_R - \vec{r}_T\,|, \qquad (3)$$

$$\vec{n} = 1/D\,(\vec{r}_R - \vec{r}_T), \qquad (3a)$$

between transmitter and receiver defines the running time t_D by integrating

$$\frac{d\vec{s}}{dt} = \vec{v}_{rel}(\vec{r}(s),t_o) + c_S\,\vec{n} \qquad (4)$$

along

$$\vec{r}(s) = \vec{r}_T + s\,\vec{n},\ 0 \le s \le D \qquad (4a)$$

which leads to

$$t_D = \int_0^D \frac{ds}{c_S + V_{rel}(s)},\ \vec{V}_{rel}\,\vec{n} = V_{rel}(s) \qquad (5)$$

The arc length s parameterises the path of the signal from the transmitter point $\vec{r}_T = \vec{r}(0)$ to the receiver point $\vec{r}_R = \vec{r}(D)$. The constant time $t = t_o$ in Eq. (4) indicates that the fluid is assumed to be frozen. The assumption is justified as long as changes in the flow pattern are small during the interval t_D, in which the signal travels through the fluid.
With

$$t^\circ_D := D/c_S \qquad (6)$$

as the running time of the signal in the fluid at rest, the running-time shift Δt is defined by

$$\Delta t := t_D - t^\circ_D. \qquad (7)$$

Δt is exactly the physical variable, which originates from experiments with ultrasonic pulses as well as from the corresponding theoretical predictions and reflects basic physical properties of the flow field.

A simple numerical example serves to estimate the order of magnitude of Δt. We consider a profile in uniform flow u_o with a small angle of incidence α relative to the flow direction. The direction of the pulse is assumed to be perpendicular to the chord of the profile and therefore the pulse propagates at a velocity c_S diminished roughly by $u_o \sin\alpha$.
For

velocity of sound	c_S	= 340 m/s
distance	D	= 0.5 m
flow velocity	u_o	= 10 m/s
angle of incidence	α	= 6°

with $\sin\alpha \simeq \alpha \simeq 0.1^r$ are

D/c_S	t°_D	= 1.4706 ms
$D/(c_S-u_o\sin\alpha)$	t_D	= 1.4749 ms
shift $t_D-t^\circ_D$	Δt	= 4.338 μs

We recognise that the running-time shift is of the order of some microseconds and is about 10^{-3} smaller than the running time itself. The magnitude estimated for Δt will reappear in almost all experiments discussed below. It should be noted that the test setup is very sensitive to a variation of D. A change ΔD of D due to an elastic deformation of the transmitter/receiver support by the fluid will alter the result for Δt significantly, if we are not aware of it.

Let

$$D' = \Delta D + D, \quad \Delta D = 0.001 \text{ m}$$

and the change be continuously recorded by a suitable ranging device. Then

$$\Delta t' = t_{D'} - t^\circ_{D'} = 4.347 \ \mu s$$

is negligibly different from Δt. If, however, the change remains unnoticed - the support is merely assumed to be rigid - then the result

$$\Delta t'' = t_{D'} - t^\circ_D = 7.288 \ \mu s$$

is wrong and measurements may lead to a misinterpretation.

The outlined problem is tractable behind fixed wings by means of a sufficiently rigid support. The first experiment with a rotating system (a wind turbine of 4 m diameter) recently performed at the author's institute showed that a continuous measurement of D together with Δt is desirable. The long extensions (Fig. 1) for the transmitter/receiver support can hardly be fixed for distances of more than about one meter.

III. Running-Time Measurements

Fig. 3 and 4 show Engler's running-time measurements and the corresponding theoretical predictions. The average accuracy of the experiments is about ± 0.1 μs. The limited accuracy is not due to the electronic equipment, but is mainly caused by asymmetries in wind tunnel flow. The experiments were conducted in the 3 x 3 m^2 Low-Speed Wind Tunnel at the DFVLR in Göttingen with an onset velocity of u_o = 20 m/s. The NACA0010 profile is suspended from three wires and connected to the model at the points P_1, P_2 and P_3 (Fig. 5). The aspect ratio is 5. For two angles of incidence 4° and 8° values of Δt are given one chord length (x/c = 1.0) behind the trailing edge.

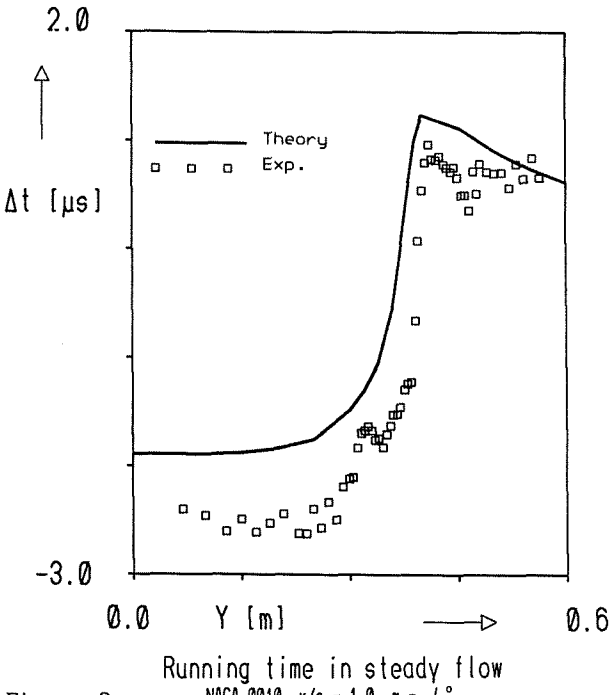

Figure 3.

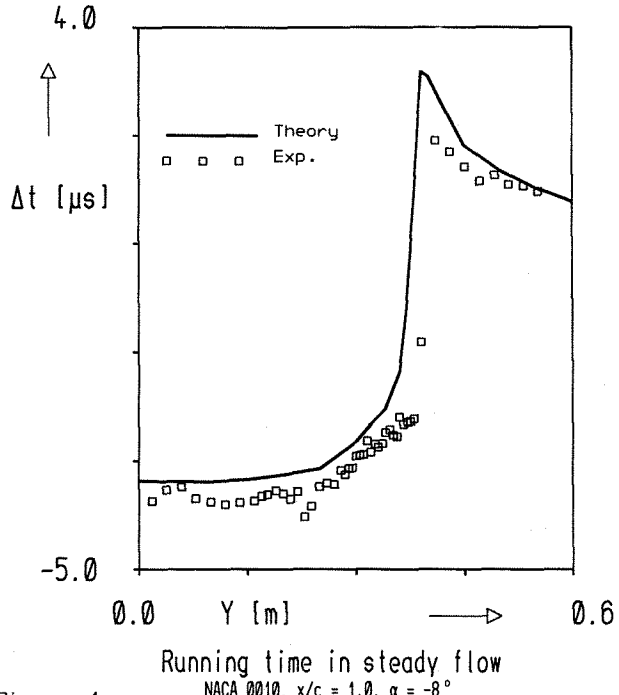

Figure 4.

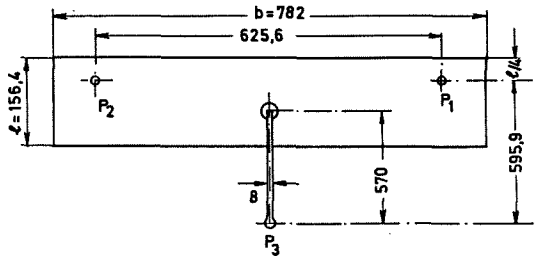

Figure 5. Geometry of Engler's NACA0010 profile (dimensions in mm)

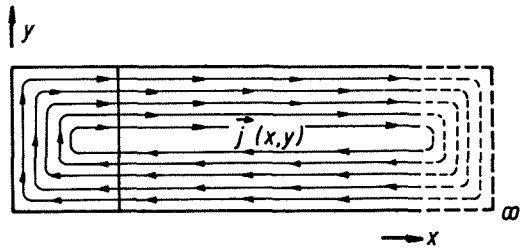

Figure 6. Vorticity in steady flow

The beam of the pulse is perpendicular to the wake and y varies from the halfspan of the profile (y = 0 m) to the tip (y = 0.39 m). The theoretical model adopts the distribution of vorticity $\vec{j}$ in a plane wake with prescribed geometry (Fig. 6).

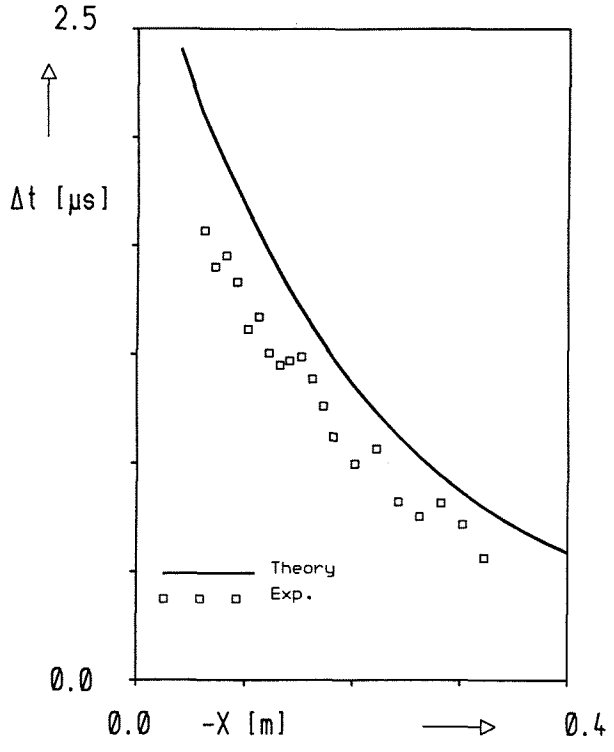

Figure 7.

The prediction of Δt also agrees fairly well with measurements in front of the profile (Fig. 7). However, there is no vorticity at all.

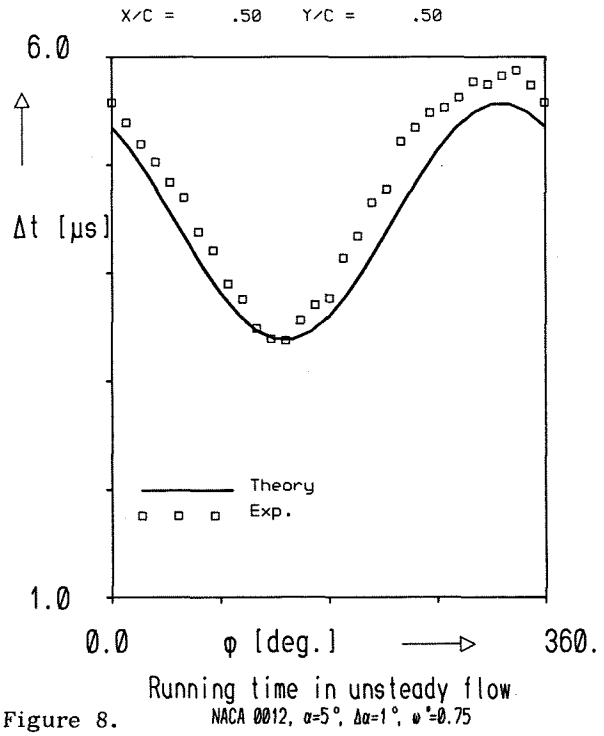

Figure 8.

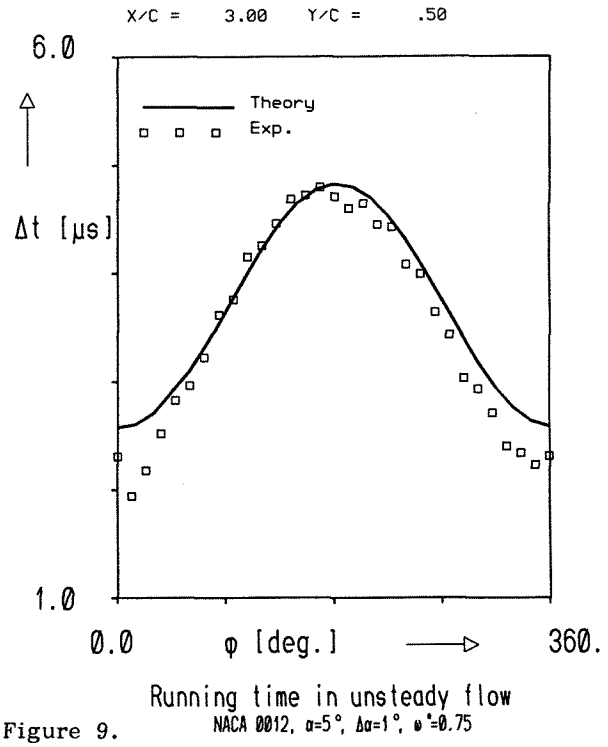

Figure 9.

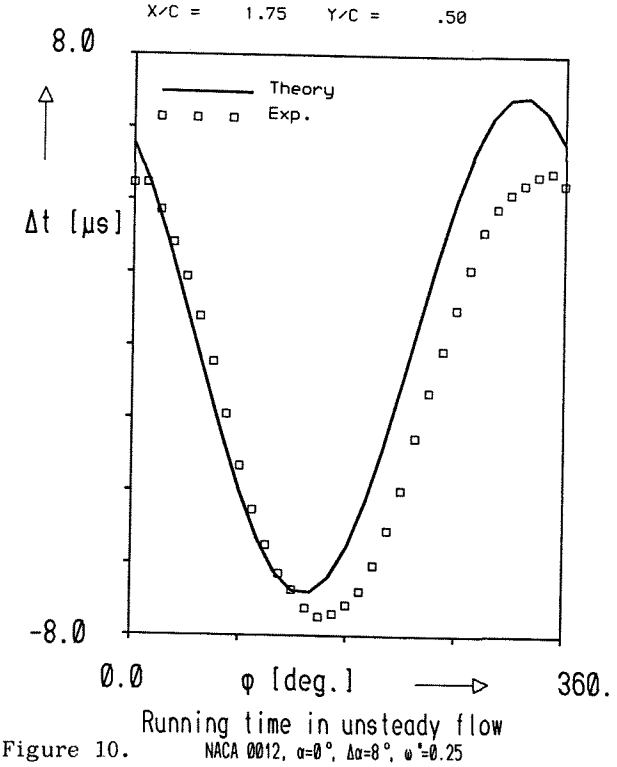

Figure 10. NACA 0012, $\alpha=0°$, $\Delta\alpha=8°$, $\omega^*=0.25$

Measurements of the unsteady case were performed by W.J. Wagner[5] at a NACA0012 half model with a chord length of 0.4 m and a span of 0.8 m. The model was mounted on a splitter plate to achieve nearly two-dimensional flow on one side. Theoretically, the model was treated as a freestream model with an aspect ratio of 4. Some of the results are yet unpublished. Selected data are presented in (4) and (5). Three typical results are shown in Fig. 8 to 10. Data are given for two different frequencies 4 and 12 Hz. In the 12 Hz case ($\omega^* = 0.75$) the downstream positions $x/c = 0.5$ and $x/c = 3.0$ are compared. The variation of Δt during one cycle of a pitching motion at a fixed position is plotted. The spanwise position is half a chord length inside the wake. The tip is located at $y = 0$. The amplitude $\Delta\alpha$ is 1° and the steady angle of incidence is 5°. Fig. 9 exemplifies the influence of a large amplitude. The 4 Hz case ($\omega^* = 0.25$) has zero angle of incidence and an amplitude of $\Delta\alpha = 8°$. The predicted running-time shift differs considerably from the experimental results. The wake is presumably distorted.

The basic ideas to understand unsteady wakes originate from L. Prandtl. The upper part of Fig. 11 is taken from his famous paper[10] given at Innsbruck in 1922. The lower part extends these ideas to three dimensions[7]. The drawing shows the vortex lines of the unsteady vorticity corresponding to Fig. 6 in steady flow. Placing the thumb of the right hand on the vertical vortex lines, the bent fingers point into the direction of the flow field. The alternating flow lines indicate unsteady lift.

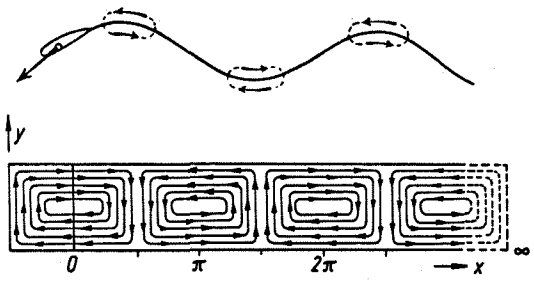

Figure 11. Vortex lines in unsteady flow

IV. Vorticity Measurements

Forming the gradient of t_D in Eq. (5) with respect to the argument $\vec{r}$ (cf. Eq. (1)) leads to

$$\operatorname{grad} t_D = \int_0^D \operatorname{grad}\left\{\frac{1}{\vec{V}_{rel}(\vec{r}(s))\,\vec{n} + c_S}\right\} ds$$

$$= -\frac{1}{c_S^2}\int_0^D \left\{1 + 2\frac{V_{rel}}{c_S} + \frac{V_{rel}^2}{c_S^2}\right\}^{-1} \times\left[(\vec{n}\,\operatorname{grad})\,\vec{V}_{rel} + \vec{n}\times\operatorname{rot}\vec{V}_{rel}\right] ds \qquad (8)$$

Measurements in air at rest differ from those in a wind tunnel merely by an uniform onset velocity u_o. Therefore, the vectorial derivatives of $\vec{v}_{rel}$ are allowed to be replaced by the derivatives of the induced velocity $\vec{v}$. Of course, the substitution does not hold in rotating coordinate systems where the kinematic part of $\vec{v}_{rel}$ does not vanish but contributes to rot $\vec{v}_{rel}$ (with a constant vector in uniformly rotating systems).

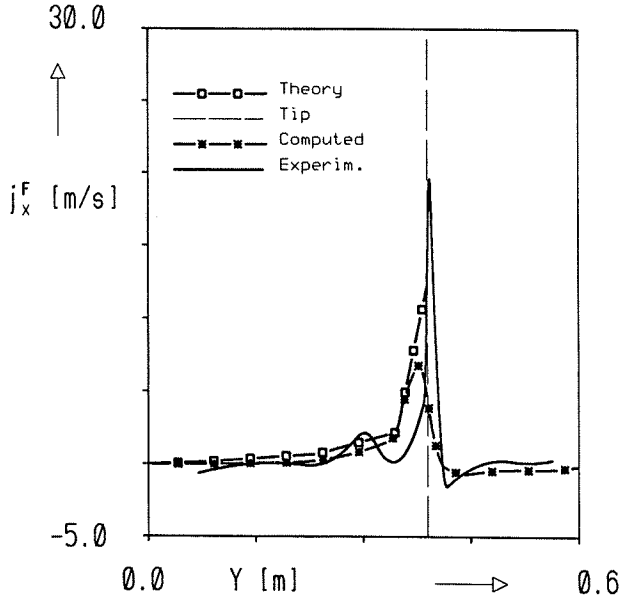

Vorticity $j_x^F(\Delta t)$
NACA 0010, x/c = 1.0, α = -4°

Figure 12.

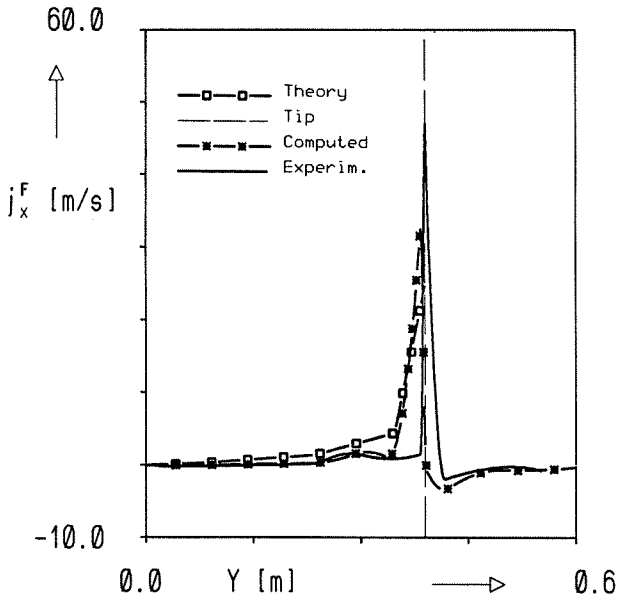

Vorticity $j_x^F(\Delta t)$
NACA 0010, x/c = 1.0, α = -8°

Figure 13.

The induced velocity $\vec{v}$ depends on the vorticity vector $\vec{j}$ by

$$\vec{V}(\vec{r},t) = \frac{1}{4\pi} \iiint_B \vec{j}(\vec{r}',t) \times \frac{\vec{r} - \vec{r}'}{|\vec{r} - \vec{r}'|^3} \, db' \quad (9)$$

We take the **first step** in approximating Eq. (8) by assuming small relative velocities compared to the velocity of sound

$$\left| 2 \frac{V_{rel}}{c_S} \right| \ll 1 \quad (10)$$

Hence Eq. (8) reads

$$\text{grad } t_D \simeq \frac{-1}{c_S^2} \int_0^D \left[(\vec{n} \text{ grad}) \vec{V} + \vec{n} \times \vec{j} \right] ds \quad (11)$$

From these three components we select the y-component for our further discussion.

$$\frac{\partial}{\partial y} t_D = - \frac{1}{c_S^2} \int_0^D \left[\frac{\partial V_y(\vec{r}',t)}{\partial z} + j_x(\vec{r}',t) \right] dz' \quad (12)$$

$$\simeq \frac{t_D(x,y+\Delta y,t) - t_D(x,y,t)}{\Delta y}$$

The y-component is the derivative of t_D in the direction of running-time measurements in the previous chapter.

Δy is the distance between two subsequent points of the measurement. It should be noted that $\vec{j}$ is the spatial distribution of vorticity and possesses the unit s^{-1}. It is not to be confused with the vorticity on an infinitely thin sheet of vorticity which has the unit m/s. We know that the spatial vorticity is spread over a more or less small boundary layer. To relate the spatially distributed vorticity to the assumed infinitely thin vortex sheet (cf. Fig. 6) we define as the total vorticity per square unit:

$$j_x^F(x,y,t) := \int_0^D j_x(\vec{r}',t) \, dz' \quad (13)$$

Resolving Eq. (12) for j^F_x we obtain

$$- \frac{1}{c_S^2} j_x^F \simeq \frac{t_D(x,y+\Delta y,t) - t_D(x,y,t)}{\Delta y} + \frac{1}{c_S^2} \left[V_y(\vec{r}_R,t) - V_y(\vec{r}_T,t) \right] \quad (14)$$

The relation between vorticity and running time still implies that the velocity field v_y is known at the respective locations of the transmitter and the receiver. However, at this step of approximation, Eq. (11) provides a relation between running time and vorticity

which holds for the steady and the unsteady case:

$$j_x^F(x,y,t) = -\left[V_y(\vec{r}_R,t) - V_y(\vec{r}_T,t)\right] - \frac{c_S^2}{\Delta y}\left[t_D(x,y+\Delta y,t) - t_D(x,y,t)\right]$$

$$j_y^F(x,y,t) = -\left[V_x(\vec{r}_R,t) - V_x(\vec{r}_T,t)\right] + \frac{c_S^2}{\Delta x}\left[t_D(x+\Delta x,y,t) - t_D(x,y,t)\right] \qquad (15)$$

Certainly some difficulties will occur when t_D, v_x and v_y are to be measured at the same time and at the same place. The difficulties may be overcome in different ways.

One solution is to replace the actual values of $\vec{v}(\vec{r}_T,t)$ and $\vec{v}(\vec{r}_R,t)$ by theoretical considerations or previously measured values. The most important aspect of latter equation is, however, that we are able to predict the error we make by omitting these additional terms.

We take the **second step** in approximating Eq. (8) by assuming negligible influence of the induced velocities at the locations of transmitter and receiver. We obtain

$$j_x^F(x,y,t) \simeq -\frac{c_S^2}{\Delta y}\left[t_D(x,y+\Delta y,t) - t_D(x,y,t)\right]$$

$$j_y^F(x,y,t) \simeq +\frac{c_S^2}{\Delta x}\left[t_D(x+\Delta x,y,t) - t_D(x,y,t)\right] \qquad (16)$$

The effect of the two steps of approximation is investigated in a mathematical model. The results are presented on the following two pages in Fig. 14.1 to 14.6 and 15.1 to 15.4. With respect to Fig. 6 the vorticity has been computed for an infinitely thin plate of aspect ratio 5 and chord length 1. The distribution of vorticity in chordwise direction has been computed by solving the corresponding integral equation as described in (6). In spanwise direction only one panel has been admitted which leads to a linear variation of j_x^F at the trailing edge. The tip is located at $y = 5$. Besides the function $j^F{}_x(y)$ plotted as a solid line in the interval from 2.5 (halfspan) to 6 (outside the wake), two types of computations in the resulting flow field are shown:

***** Asterisks
first step of approximation with $j^F{}_x$ according to Eq. (14)

□□□□ Squares
second step of approximation with $j^F{}_x$ according to Eq. (16)

In Fig. 14 the values are taken 1/10 chord length behind the plate, in Fig. 15 1/10 chord length ahead of the plate upstream. The three rows of figures differ in their distance D between "transmitter" and "receiver", which are placed D/2 perpendicular to the plane of the wake above and below, respectively. In the first row D is 1 chord length, D = 2 chord lengths in the second row and D = 6 chord lengths in the third row.

The computations show very clearly that a distance of 6 chord lengths is sufficient to obtain satisfactory results for the vorticity distribution, though the induced velocity is not taken into account. In Fig. 15 the question is answered whether changes in the running time might feign a presence of vorticity where no vorticity is supposed to be at all. The $j^F{}_x$-curve in Fig. 15, of course, has no meaning with respect to the computed values. It is kept in the figures for comparison of the computed error with the absolute magnitude of the present vorticity.

Fig. 12 and 13 show the vorticity distribution resulting from Fig. 3 and 4 (Engler's NACA0010 profile in steady flow). When the experiments were conducted seven years ago, the results were not intended to be applied for predictions of vorticity distributions. The distance D is about 3 chord length in all experiments. Unfortunately no experiments were planned up to now with an appropriate test setup to check the theoretical considerations. However, the results in these two figures look quite promising.

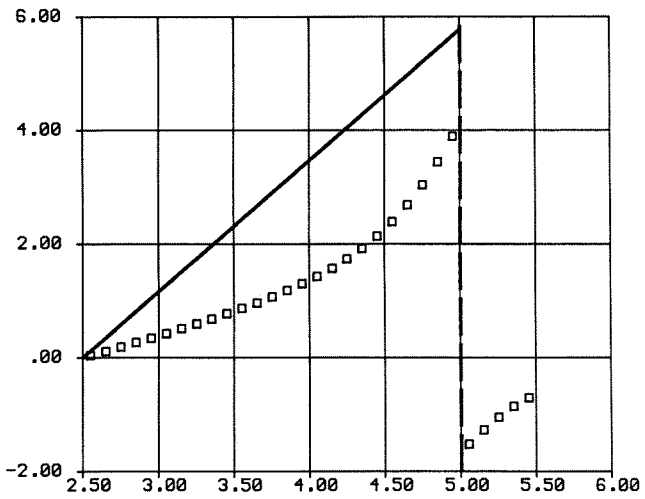

Figure 14.1 $j^F_x(y)$, D/c=1, without v_y

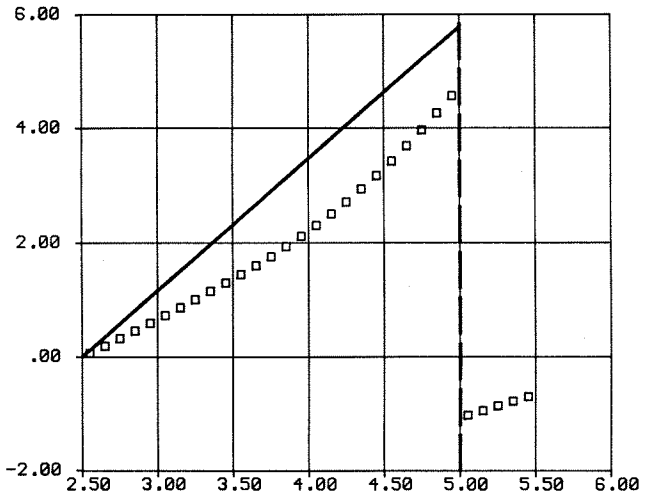

Figure 14.2 $j^F_x(y)$, D/c=2, without v_y

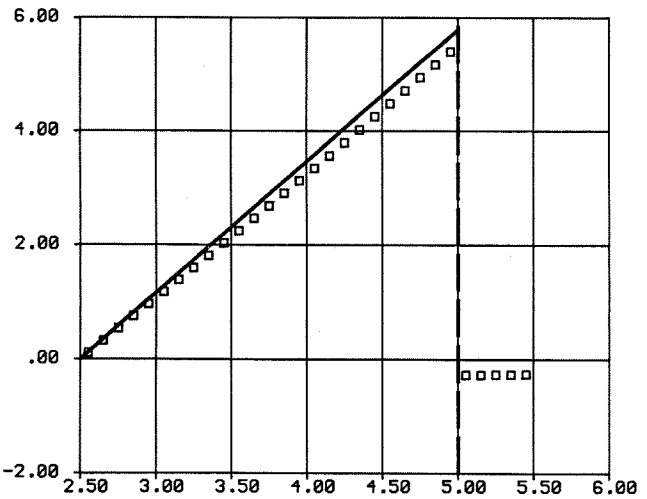

Figure 14.3 $j^F_x(y)$, D/c=6, without v_y

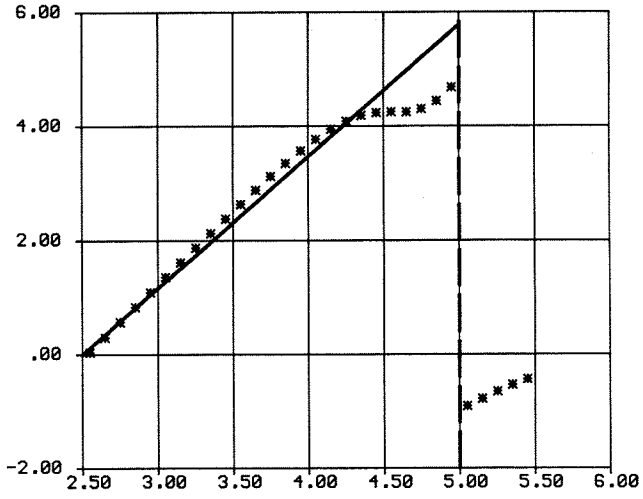

Figure 14.4 $j^F_x(y)$, D/c=1, with v_y

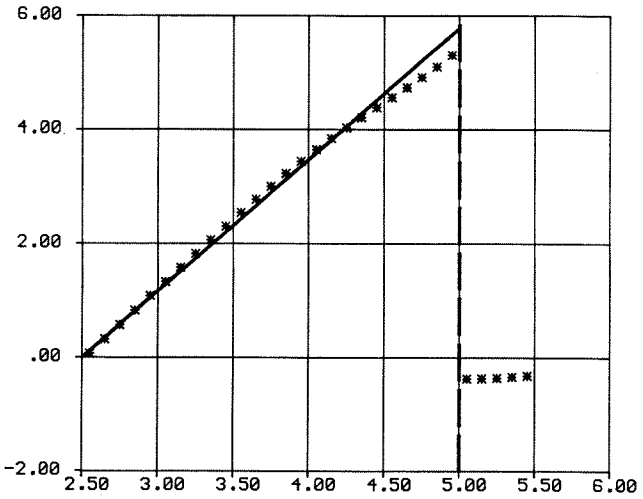

Figure 14.5 $j^F_x(y)$, D/c=2, with v_y

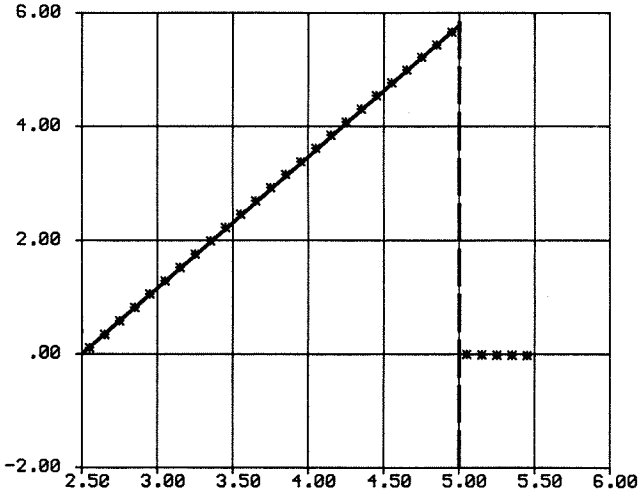

Figure 14.6 $j^F_x(y)$, D/c=6, with v_y

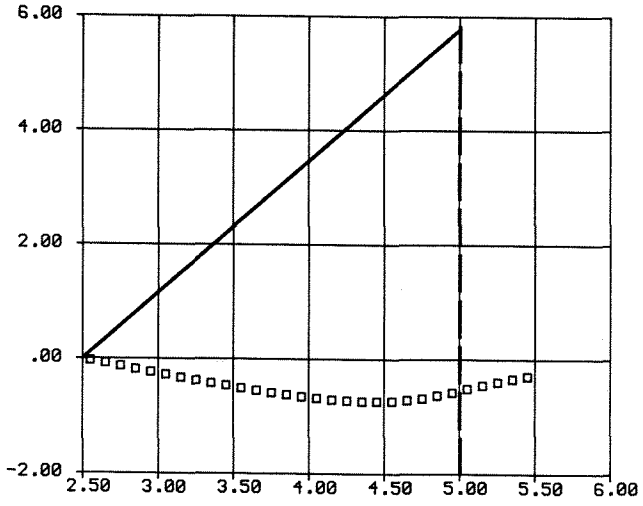

Figure 15.1 $j^F{}_x(y)$, D/c=1, without v_y

The broken line filled in with squares shows the vorticity distribution along the trailing edge according to the solution of the integral equation. The broken line with asterisks is the vorticity distribution computed from the induced flow field without taking the v_y term into account (second step). The solid line is the vorticity taken from the interpolated experimental running-time data. It should be noted that there is a certain degree of freedom to interpolate the data.

V. Prediction of Lift

The vorticity in a flow field is closely related to the circulation integral. In the present case vorticity in the flow field is confined to a rather thin boundary layer originating from the profile.

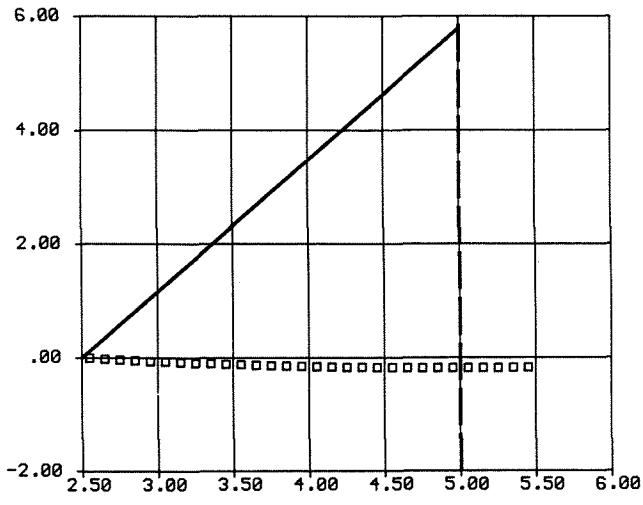

Figure 15.2 $j^F{}_x(y)$, D/c=6, without v_y

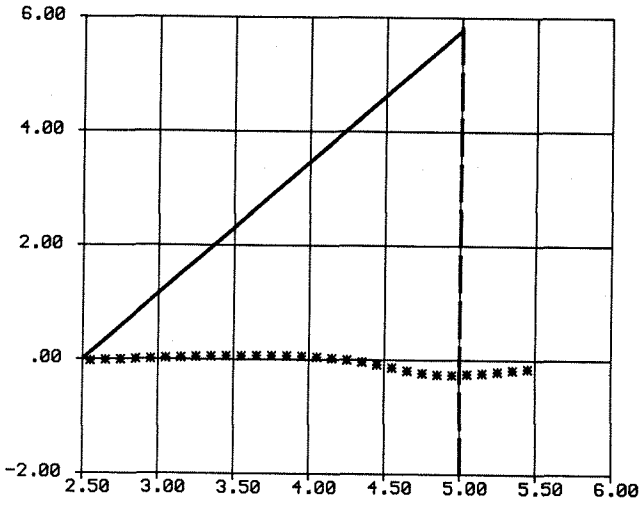

Figure 15.3 $j^F{}_x(y)$, D/c=1, with v_y

In general the circulation of a two-dimensional domain B is given by

$$\Gamma(t) = \oint_{\partial B} \vec{V}(\vec{r}(s),t)\, d\vec{r}(s) = \iint_B \mathrm{rot}\, \vec{V}\, dF = \iint_B \vec{j}\, d\vec{F} \qquad (17)$$

If the domain of nonvanishing vorticity within B is confined to an infinitely thin sheet, the computation of circulation reduces to a line integral. If B encloses the profile precisely in the plane of symmetry, the integral has to be taken along the chord

$$\Gamma(t) = \int_0^C j_y^F(x,0,t)\, dx \qquad (18)$$

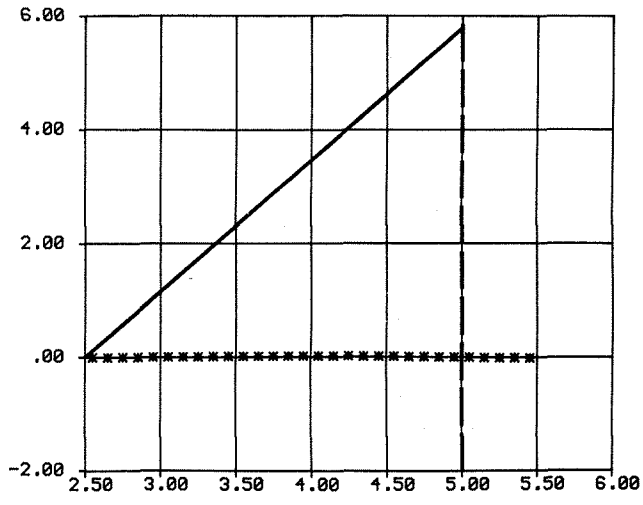

Figure 15.4 $j^F{}_x(y)$, D/c=6, with v_y

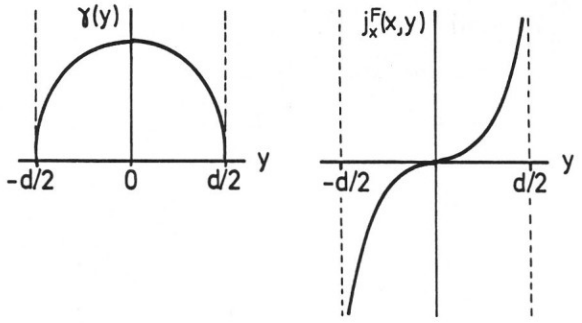

Figure 16. Spanwise distribution of circulation and vorticity

The result of Eq. (18) is completely equivalent to an integration over the spanwise distribution of the downstream-flowing vorticity $j^F{}_x(y)$ along the trailing edge:

$$\Gamma(t) = \int_0^{d/2} j_x^F(x,y,t)\, dy \qquad (19)$$

$$x \geq c \ .$$

The spanwise distribution of lift is proportional to $\gamma(y)$ and is obtained from the vorticity measurement by

$$\gamma(y,t) = \Gamma(t) - \int_0^{y} j_x^F(x,y',t)\, dy' \qquad (20)$$

$$x \geq c$$

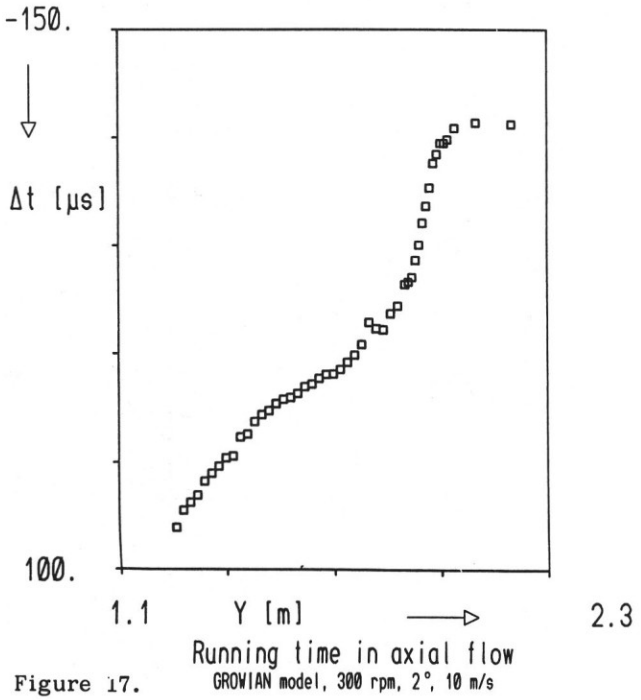

Figure 17.

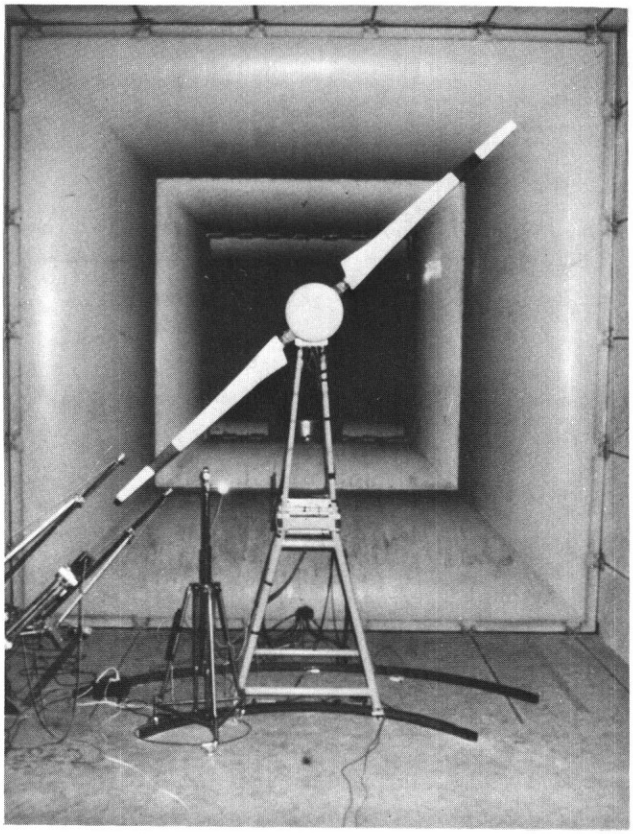

Figure 19. Wind tunnel test setup for measurements of running times in rotating systems

The dependence of time t in the preceding equations holds, of course, only for the limiting case of small reduced frequencies. The more general case of harmonic oscillations has to be treated according to Eq. (16).

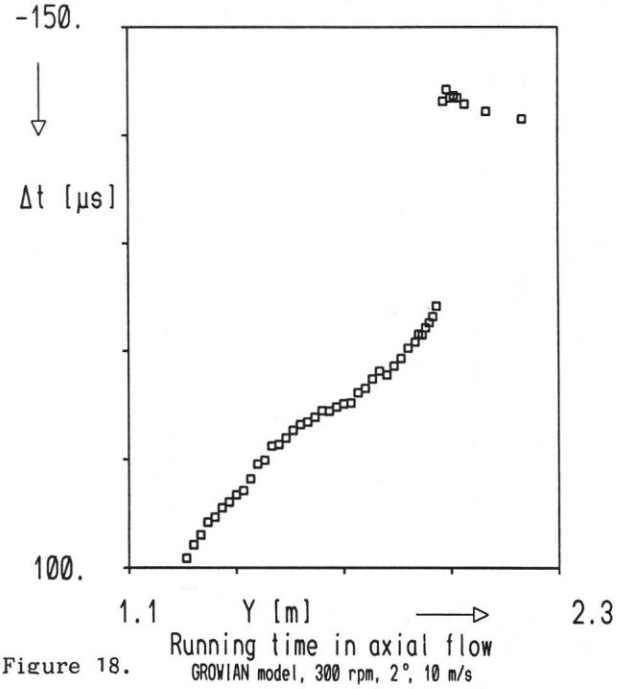

Figure 18.

However, the reduction of measured vorticity to unsteady lift remains a theoretical work which still has to be done.

VI. Further Development

The first runnig-time measurements for a rotating system were begun recently[11]. The wind tunnel test setup can be seen in Fig. 19. The lack of a laser-beam guided ranging device is obvious. Work is done on this subject presently by R. Engler[12]. Fig. 17 and 18 show running-time measurements in a rotating system. The support for transmitter and receiver covers the outer part of the rotor disc with a diameter of 4 m. Fig. 17 displays values just behind the trailing edge. In Fig. 18 the vortex of the preceding blade crosses the test section.

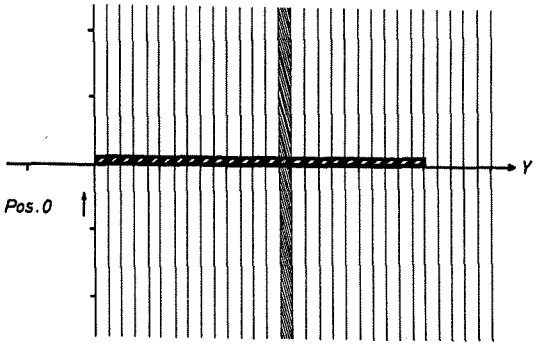

Figure 20. 2-D spatial resolution

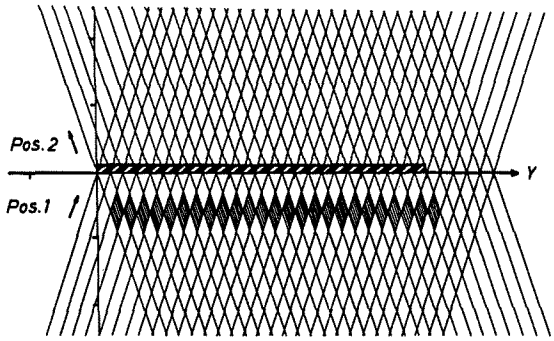

Figure 21. 3-D spatial resolution

Finally Fig. 20 and 21 show how a three-dimensional resolution of the wake formation can be handled. Eq. (14) is independent of the direction of the beam provided that the region of nonzero vorticity is concentrated in a thin sheet, the position of which is to be traced. The third dimension in Fig. 21 is given by the downstream location of the support.

VII. References

(1) D.W. Schmidt, Akustische Messung der Zirkulation von Wirbeln und Zirkulationsverteilungen bei Modelluntersuchungen in Windkanälen, Mitt. MPI für Strömungsforschung und AVA, Nr. 61, Göttingen 1975

(2) R.H. Engler, Untersuchungen von Randwirbeln mittels Ultraschall im Nahbereich hinter einem Rechteckflügel im Windkanal, MPI für Strömungsforschung, Bericht 11/79, Göttingen 1979.

(3) R.H. Engler, W.J. Wagner, B. Weitemeier, Experimental Study of the Tip Vortices behind an Oscillating Blade by the Ultrasonic Method, Proc. of the colloquium honoring Hans Georg Küssner on the occasion of his 80th Birthday, Göttingen 1980.

(4) R.H. Engler, D.W. Schmidt, W.J. Wagner, B. Weitemeier, Ultrasonic Method for Flow Field Measurement in Windtunnel Tests, J.Acoust. Soc. Am. 71(1), 1982 pp. 42-50.

(5) W.J. Wagner, Comparative Measurements of the Unsteady Pressures and the Tip-Vortex Parameters on Four Oscillating Wing Tip Models, Tenth European Rotorcraft Forum, No. 9, The Hague 1984.

(6) W. Send, Higher-Order Panel Method Applied to Vorticity-Transport Equation, Fifth European Rotorcraft and Powered Lift Aircraft Forum, No. 16, Amsterdam 1979.

(7) W. Send, Der instationäre Nachlauf hinter schlanken Auftriebskörpern in inkompressibler Strömung, ZAMM 64, 1984, S. 7-15.

(8) W. Send, Analytical Representation of the Three-Dimensional Wake Integral in Unsteady Flow, Proc. of the colloquium honoring Hans Georg Küssner on the occasion of his 80th Birthday, Göttingen 1980.

(9) W. Send, Theoretical Prediction of Running-Time Measurements in Unsteady Flow, Tenth European Rotorcraft Forum, No. 15, The Hague 1984.

(10) L. Prandtl, Über die Entstehung von Wirbeln in der idealen Flüssigkeit, mit Anwendung auf die Tragflügeltheorie und andere Aufgaben, in: Th.v. Karman und T. Levi-Civita, Vorträge aus dem Gebiet der Hydro- und Aerodynamik (Insbruck 1922), Springer Verlag, Berlin 1924.

(11) W.J. Wagner, L. Deppe, Investigations for enhancing the performance of windmills, DFVLR Göttingen, to be published.

(12) R.H. Engler, Development of a laser-beam guided ranging device for running-time measurements, DFVLR Göttingen, part of a Ph.D. Thesis, to be published.